



# Performance of quartz- and sapphire-based double-crystal high-resolution ( $\sim 10$ meV) RIXS monochromators under varying power loads

Thomas Gog,<sup>a\*</sup> Diego M. Casa,<sup>a</sup> Jonathan Knopp,<sup>a</sup> Jungho Kim,<sup>a</sup> Mary H. Upton,<sup>a</sup> Richard Krakora,<sup>a</sup> Alan Jaski,<sup>a</sup> Ayman Said,<sup>a</sup> Hasan Yavaş,<sup>b</sup> Hlynur Gretarsson<sup>c</sup> and Xian Rong Huang<sup>a</sup>

Received 25 February 2018

Accepted 17 April 2018

Edited by M. Eriksson, Lund University, Sweden

**Keywords:** X-ray optics; resonant inelastic X-ray scattering; RIXS; non-traditional crystal materials; high-resolution monochromators.

**Supporting information:** this article has supporting information at journals.iucr.org/s

<sup>a</sup>Advanced Photon Source, Argonne National Laboratory, 9700 South Cass Avenue, Lemont, IL 60439, USA,

<sup>b</sup>Deutsches Elektronen Synchrotron DESY, Notkestrasse 85, 22607 Hamburg, Germany, and <sup>c</sup>Max-Planck-Institut fuer Festkoerperforschung, Heisenbergstrasse 1, 70569 Stuttgart, Germany. \*Correspondence e-mail: gog@anl.gov

In the context of a novel, high-resolution resonant inelastic X-ray scattering spectrometer, a flat-crystal-based quartz analyzer system has recently been demonstrated to provide an unprecedented intrinsic-energy resolution of 3.9 meV at the Ir  $L_3$  absorption edge (11.215 keV) [Kim *et al.* (2018) *Sci. Rep.* **8**, 1958]. However, the overall instrument resolution was limited to 9.7 meV because of an 8.9 meV incident band pass, generated by the available high-resolution four-bounce Si(844) monochromator. In order to better match the potent resolving power of the novel analyzer with the energy band pass of the incident beam, a quartz(309)-based double-bounce, high-resolution monochromator was designed and implemented, expected to yield an overall instrument resolution of 6.0 meV. The choice of lower-symmetry quartz is very attractive because of its wealth of suitable near-backscattering reflections. However, it was found that during room-temperature operation typical levels of incident power, barely affecting the Si monochromator, caused substantial thermal distortions in the first crystal of the quartz monochromator, rendering it practically unusable. Finite-element analyses and heat-flow analyses corroborate this finding. As a high-flux, lower resolution (15.8 meV) alternative, a two-bounce sapphire(078) version was also tested and found to be less affected than quartz, but notably more than silicon.

## 1. Introduction

The development of crystal-based high-energy-resolution X-ray optics employing materials other than the traditional ‘ideal crystal’ silicon has received much attention in the last few years (Yavaş *et al.*, 2017). For resonant techniques such as resonant inelastic X-ray scattering (RIXS), where the incident energy is predetermined by the selected absorption edge, lower-symmetry crystals such as trigonal quartz and sapphire offer many more highly resolving, near-backscattering Bragg reflections than the higher-symmetry cubic zinc blende crystals such as Si, Ge and the III–V semiconductors. In addition, near-perfect single-crystal quartz in large sizes is now available commercially (Gog *et al.*, 2013; Sutter *et al.*, 2005, 2006; Honnicke *et al.*, 2013; Said *et al.*, 2018). RIXS in particular is striving for energy resolutions in the sub-10 meV regime (Ament *et al.*, 2018). In this regard, a flat-crystal-based quartz(309) analyzer system was recently demonstrated with an intrinsic energy resolution of 3.9 meV at the Ir  $L_3$  absorption edge (11.215 keV) (Kim *et al.* 2018). This is unprecedented for a RIXS analyzer. However, the overall resolution of the entire RIXS spectrometer was only 9.7 meV, primarily

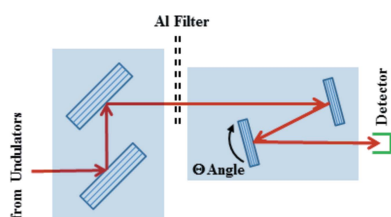


**Table 1**  
Thermal properties of quartz, sapphire and silicon.

	Thermal conductivity ( $\text{W m}^{-1} \text{K}^{-1}$ ) <sup>†</sup>		Thermal expansion ( $10^{-6} \text{K}^{-1}$ ) <sup>†</sup>	
	to c-axis	⊥ to c-axis	to c-axis	⊥ to c-axis
Quartz‡	10.7	6.2	7.1	13.2
Sapphire‡	23.1	25.2	6.66	5.0
Silicon‡	149		2.6	

<sup>†</sup> At room temperature. <sup>‡</sup> Data for quartz obtained from <http://www.crystran.co.uk/optical-materials/quartz-crystal-sio2>; for sapphire: [http://www.mt-berlin.com/frames\\_cryst/descriptions/sapphire.htm](http://www.mt-berlin.com/frames_cryst/descriptions/sapphire.htm); for silicon: <http://en.wikipedia.org/wiki/Silicon>.

limited by the only available choice of high-resolution monochromator, namely a four-bounce Si(844), with a band pass of 8.9 meV. Thanks to the availability of suitable near-backscattering reflections, a two-bounce monochromator with symmetric quartz(309) crystals could be devised. The expected band pass was 4.6 meV, which would result in an overall energy resolution of 6.0 meV, a much better match to the analyzer resolution. No Si reflection exists that can deliver the same resolution in a two-bounce setting. However, during room-temperature operation it became evident that the thermal distortions of the first quartz crystal caused by typical levels of incident power, which barely affect Si monochromators, were so severe that ultimately no exit beam with usable intensity and energy resolution could be generated. These experimental findings were subsequently confirmed by finite-element analysis (FEA) and thermodynamic considerations, leading to the conclusion that the thermal conductivity is too poor to allow quartz X-ray optics to be used in high-power, high-resolution applications.

Using the same instrumentation and experimental conditions, a set of sapphire(078) crystals were also tested with the aim of providing a higher-flux, lower-resolution alternative with 15.3 meV intrinsic and 16.4 meV overall resolution. In actual operation, the thermal distortion of the first sapphire crystal was much less severe than in quartz, but still noticeably more than for silicon. This finding is intuitively consistent considering the thermal conductivities of quartz, sapphire and silicon, combined with their thermal expansions at room temperature as indicated in Table 1. It should be noted that data on material properties quoted in the literature, especially for quartz and sapphire, are widely scattered (Sutter & Yavas, 2017). Thus, calculations performed for this article are more of a qualitative than a precise quantitative nature.

## 2. Experimental

The present study was conducted at the RIXS beamline 27-ID at the Advanced Photon Source (APS) at Argonne National Laboratory. An independent attempt to implement a quartz-based monochromator was also made at beamline P01 at PETRA III at DESY by two co-authors of the present study (HY and HG); however, as a result of the irreversible damage to the crystals during testing, experimental data gathered are limited.

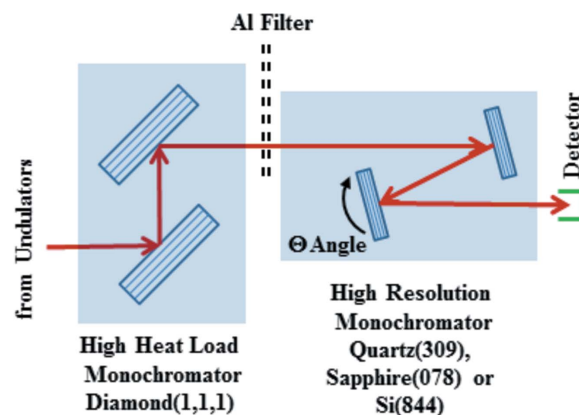


**Figure 1**  
Dispersive arrangement of the HHL and high-resolution monochromators. Aluminium filters could be inserted between the two devices to reduce the power on the high-resolution monochromator.

At the APS, undulator radiation at 11.215 keV, originating from two 2.4 m-long, 30 mm in-line insertion devices, was incident on a combination of a water-cooled, double-crystal diamond(111) high-heat-load (HHL) monochromator, succeeded by an in-air or in-He, double-crystal high-resolution monochromator. The latter could be equipped with sets of individual quartz(309), sapphire(078) or Si(844) crystals. HHL and high-resolution monochromators were arranged in a dispersive configuration, as shown schematically in Fig. 1. The intensity from the HHL monochromator was determined to be  $3.4\text{--}5.1 \times 10^{13} \text{ photons s}^{-1}$  using a PIN diode, resulting in an incident power on the first crystal of the high-resolution monochromator of 61–92 mW. Aluminium filters of varying thickness could be inserted between the two devices to attenuate the incident power. The beam footprint on the first crystal was approximately  $0.75 \text{ mm} \times 1.5 \text{ mm}$  (v × h) FWHM.

### 2.1. Quartz(309)

Quartz crystals were manufactured from boules of very low-defect-density material supplied by MuRata (formerly Tokyo Denpa). The boules were oriented to the (309) reflection, cut into flat slabs  $\sim 15 \text{ mm} \times 20 \text{ mm} \times 2 \text{ mm}$  in size, and polished at the APS. Prior to installation, the quartz crystals were individually characterized at low-incident power. The characterization setup is shown in the inset of Fig. 2. It employed a sequence of diamond(111)–Si(844) monochromators, followed by the quartz crystal to be tested, unconstrained on a high-resolution rotation stage. Rocking curves were recorded around the Bragg angle of  $\theta = 88.36^\circ$  and compared with simulated reflectivity curves. Simulations are based on two-beam dynamical diffraction theory (Authier *et al.*, 2001; DuMond, 1937), overlaying reflectivity curves of successive optical elements in angle–energy space. In this way, the entire X-ray environment, from undulator source to detector, is taken into account. Rocking curves for the two representative quartz crystals together with the simulation are shown in the left panel of Fig. 2. All crystals tested were within 10% of

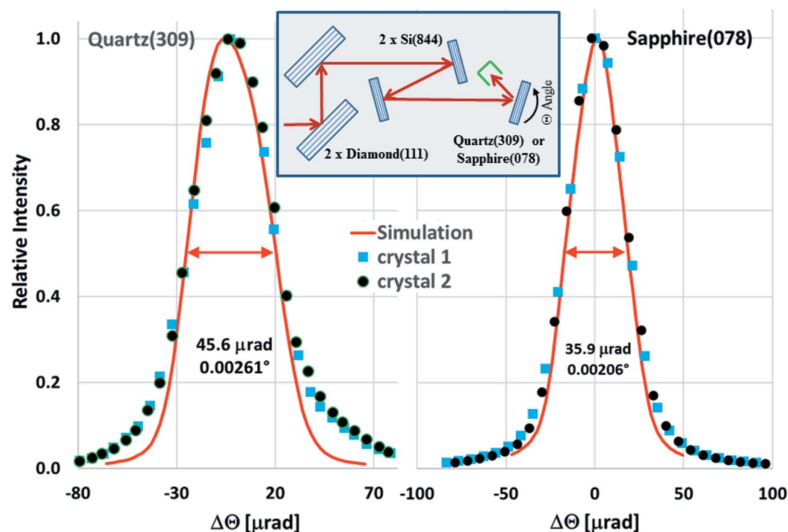


**Figure 2** Rocking curves of individual quartz(309) and sapphire(078) crystals recorded at low incident power using the setup shown schematically in the inset. Simulated curves (solid red lines) are included for comparison. All crystals tested were within 10% of the expected FWHM, although tails deviate somewhat from the simulation.

the expected FWHM, although tails deviate somewhat from the simulation; thus, the crystals were deemed to be of near-ideal quality.

The quartz crystals were mounted in the high-resolution monochromator in a strain-free fashion, using very weak leaf springs made from 25 μm-thick steel foil. The absence of mounting strain was verified by recording rocking curves of the second crystal at very low incident X-ray intensity, which exhibited widths fully consistent with the previous character-

ization and simulations. The device was then subjected to the full beam from the HHL monochromator ( $\sim 4 \times 10^{13}$  photons  $s^{-1}$ ). Measured rocking curves were almost 20 times wider than simulations, as shown in the inset of Fig. 3. It is assumed that the second crystal is not subject to a significant beam intensity since the ratio of reflected and incident intensities at the first crystal can at most be as large as the ratio of high-resolution and HHL monochromator band passes ( $4.6/\sim 800 = 6 \times 10^{-3}$ ). Consequently, the observed rocking-curve broadening was considered a measure of severe thermal strain in the first crystal. In the next step, the incident intensity was successively reduced by inserting aluminium filters while rocking curves were recorded at each point. Results are shown in Fig. 3 for two environments, namely in air and in gently flowing room-temperature He gas. Here, the broadening relative to the simulated width (reference) is graphed as a function of filter transmission. Remarkably, the incident intensity had to be reduced by almost three orders of magnitude before an acceptable width was attained. At that point, the intensity of the high-resolution beam emitted from the second crystal was too low to be of practical use for the photon-hungry RIXS technique. Also noteworthy is that an expected cooling effect from the He environment did not improve the reflection width.

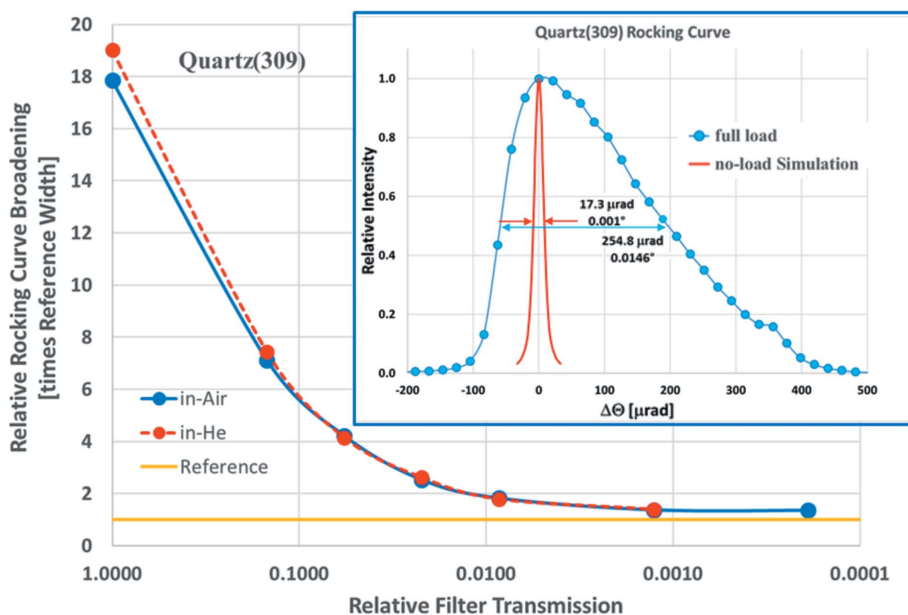


**Figure 3** Second-crystal rocking-curve widths of the high-resolution quartz monochromator as a function of incident intensity relative to the full beam from the HHL monochromator. Curves for two environments, in air and in He, are shown. The inset shows the rocking curve at full beam compared with a simulated ideal curve.

### 2.2. Sapphire(078)

Sapphire crystals were made in cooperation with Rubicon Technology, Inc. Boules of low-defect-density material were oriented to the (078) reflection. Oriented boules were then cut into 75 mm-diameter, 2 mm-thick wafers and then polished. Flat slabs of  $\sim 10$  mm  $\times$  15 mm  $\times$  2 mm in size were wire-cut from these wafers and then annealed at 1200°C for 24 h. Similar to the quartz crystals, prior to installation, the sapphire crystals were individually characterized at low incident power using the setup shown in the inset of Fig. 2. Rocking curves were recorded around the Bragg angle of  $\theta = 87.22^\circ$  and compared with simulated reflectivity curves. Results are shown in the right-hand panel of Fig. 2. Again, all crystals tested were within 10% of the expected FWHM and deemed to be of near-ideal quality.

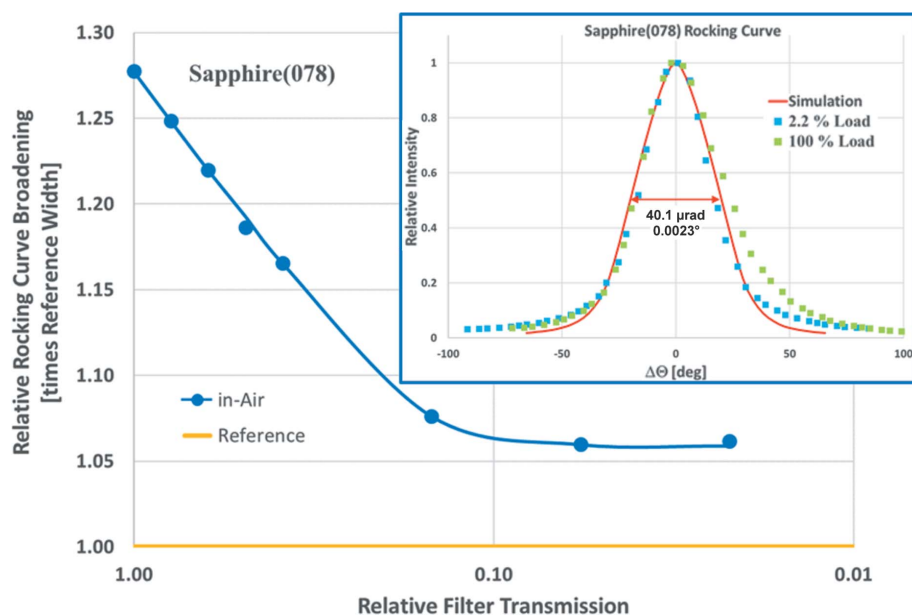


**Figure 4** Second-crystal rocking-curve widths of the high-resolution sapphire monochromator as a function of incident intensity relative to the full beam from the HHL monochromator. The inset shows the rocking curve at full beam compared with a simulated ideal curve.

The sapphire crystals were mounted in the high-resolution monochromator and strain-free conditions were verified. Subjecting the device to the full incident beam resulted in far less distortions of the crystals than for quartz, as shown in Fig. 4. The maximum rocking-curve broadening is now less than 30%, and only a light enhancement of the high-angle tail in the high-load case is observed with respect to low-load conditions.

### 2.3. Finite-element and heat-flow analysis

In order to put these measurements into context, numerical finite-element analysis (FEA) was performed for the quartz case which fully corroborated the experimental findings. Subsequently, it was found that the basic behaviour of the quartz system could also be captured by an analytical thermodynamic model of heat flow in a semi-infinite medium. This model allows us to make basic predictions for different load conditions and even other crystal materials such as sapphire and silicon based on the maximum temperature rise attributed to the power deposited into the crystal, its thermal conductivity and expansion coefficient.

For the FEA analysis, a bulk quartz crystal with the (309) direction as the surface normal was modelled using the engineering simulation program

ANSYS (version 17.2). The anisotropic properties of quartz (thermal conductivity, thermal expansion and Young's modulus) were taken into account (quartz thermal property data were taken from [www.crystran.co.uk/optical-materials/quartz-crystal-sio2](http://www.crystran.co.uk/optical-materials/quartz-crystal-sio2)). Heating caused by the incident X-ray beam was represented by a volumetric density function with Gaussian profiles along the surface and an exponential decay normal to the surface, commensurate with the attenuation length of quartz at 11.215 keV. As a thermal boundary condition, natural convection in still air at 22°C was applied to the entire crystal surface. Steady-state temperature- and strain-fields were then calculated for various levels of incident power, ranging from the highest intensity estimate ( $5.1 \times 10^{13}$  photons  $s^{-1}$  = 92 mW) down a list of attenuation values similar to those used in measurements. In order to convert the data obtained to simulated

rocking curves that can be compared with measurements, further processing was performed with the symbolic computation program *Mathematica* (version 11.0). The inset in Fig. 5 shows the field of strains normal to the surface at full power in the region of the beam footprint. These strains are directly related to local deviations in diffraction plane spacing,  $\Delta d/d$ ,

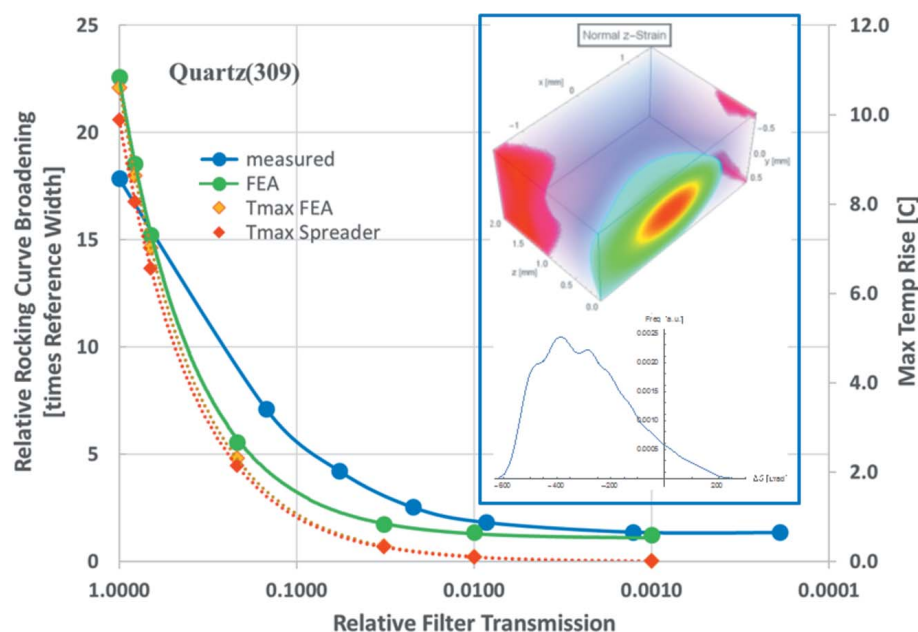


**Figure 5** Quartz rocking-curve broadening (left axis) estimated by FEA (green) compared with measurements in air (blue). Also plotted are the maximum temperature rises (right axis) calculated by FEA (orange) and by the spreader model (red). Inset: FEA volumetric normal strain profile for quartz at full load near the beam center. Asymmetries are caused by the anisotropy in both thermal conductivity and expansion coefficient. Below, a histogram of the weighted distribution of Bragg angle displacements.

which in turn, by virtue of Bragg's law, results in local deviations of the Bragg angle of  $\Delta\theta = (\Delta d/d) \tan \theta_B$ . Here  $\theta_B$  is the Bragg angle in the absence of strain. Each point is now assigned a weight proportional to the incident power density multiplied by an additional absorption factor to account for the reflected beam exit path through the crystal. The resulting distribution for full power is also shown in the inset of Fig. 5, displaying an asymmetric shape quite reminiscent of the measured rocking curve shown in the inset of Fig. 3. Actual rocking-curve widths as a function of incident power were obtained by convolution of angular deviation distributions with unstrained reflectivity profiles, or estimated from a quadrature of the local deviation distribution and the width of the unstrained profile. Rocking-curve widths obtained in this way are plotted in Fig. 5 (green curve), showing that the incident-power dependence and the size of the effect of thermal distortions on crystal reflectivity closely match the measurements performed.

Additional insight can be gained from thermodynamic considerations which can help to assess the severity of thermal strain in different materials and conditions without the need for FEA simulations. The analytical model utilized here is known as an 'idealized heat spreader' (Carslaw & Jaeger, 1959). It consists of solving the heat conduction equation in steady state for a simplified case, where heat flows into an isotropic, semi-infinite medium only within a finite circular region on its surface. The poor thermal conductivity of quartz indeed allows such treatment for a crystal surface larger than the beam footprint and a thickness larger than the attenuation length; consequently surface convective effects are neglected and all heat generation is confined to the surface. Temperature profiles obtained are solutions of the Laplace equation, subject to the boundary conditions mentioned above. For a circular heat source of radius  $a$  and power  $P$ , applied to a material of isotropic thermal conductivity  $K$ , the model leads to a maximum temperature rise at the surface of

$$\Delta T_{\max} = \frac{P}{K\pi a}. \quad (1)$$

With  $K = K_z \simeq 6.42 \text{ W m}^{-1} \text{ K}^{-1}$  (Simmons, 1961) and an applied beam size of  $a = 0.451 \text{ mm}$ , the maximum temperature rise in quartz as obtained by FEA analysis and the spreader model are indeed consistent with each other, as shown in Fig. 5 by the red and orange dashed curves, respectively.

For comparison with the experimental results plotted in Figs. 3 and 4, the model yields a relative broadening of rocking curves based on the maximum temperature rise of

$$\Delta\theta_{2,\max} / \Delta\theta_{2,o} = (1 + S^2)^{1/2} \quad (2)$$

where

$$S \simeq 0.03 \frac{P}{a} \frac{\alpha \tan \theta_{B0}}{K \delta\theta}. \quad (3)$$

The first factor combines constants and numerical estimates as explained in the supporting information. The second factor depends on beam properties (power  $P$  and size  $a$ ), the third on material properties (expansion coefficient  $\alpha$  and thermal

conductivity  $K$ ) and the last on the selected reflection (nominal Bragg angle  $\theta_{B0}$  and reflection width  $\delta\theta$ ). This approximation results in values of 14 and 1.3 for quartz(309) and sapphire(078), respectively, very close to the values of 18 and 1.3 shown in Figs. 3 and 4.

#### 2.4. Quartz-based monochromator of PETRA III at DESY

An attempt to implement a quartz-based, double-crystal, high-resolution monochromator for RIXS measurements was independently made at beamline P01 of Petra III at DESY. Here the desired absorption edge was Ru  $L_3$  at 2.838 keV, and quartz(1,0,-2) crystals from the same source as above were used. Initially, measured rocking-curve widths were only mildly distorted (<20% FWHM), which can be understood by considering relative broadening of rocking curves based on the maximum temperature rise. With an incident power on the quartz crystals of about ten times smaller, the tangent of the Bragg angle about five times smaller and the intrinsic reflection width about five times larger, this broadening in the PETRA III case is quite negligible. However, at PETRA III over a period of 10 h there followed non-reversible damage to the quartz crystals of unknown origin, which rendered the monochromator unusable. No such behavior was seen at the APS, where thermal distortions vanished as soon as the incident power was removed.

### 3. Summary and outlook

In the present study, an attempt was made to harness the wealth of near-backscattering reflections in non-traditional, lower-symmetry crystal materials, such as quartz and sapphire, for a double-crystal, high-resolution RIXS monochromator at the Ir  $L_3$  absorption edge. For quartz(309) at room temperature, thermal distortions were so severe that ultimately no useful beam could be extracted. This thermal behavior was corroborated by FEA and is also consistent with estimations based on the thermodynamic heat-spreader model.

There are few options for mitigating these thermal deficiencies in quartz. Uniform cooling or heating of the quartz crystals near room temperature at any of its surfaces would only exacerbate temperature differences at best. Even some profiled heating/cooling solution would have to be very precise: alignment well within beam size (<0.1 mm), temperature differences well within 0.01 K, within beam footprint and any additional strain (from mounting heaters, etc.) well below  $\sim 10^{-7}$ . The crystals could be made smaller in order to decrease the thermal thickness. However, the lateral sizes would have to be reduced to be comparable with the beam footprint, which would imply loss of reflecting area for the beam tails and potentially strained crystal edges coming into the beam footprint. The crystal thickness could be reduced, but at values comparable with the attenuation length ( $\sim 350 \mu\text{m}$ ) it is doubtful that the crystal quality would still be sufficient. Another mitigation strategy would be to spread the beam power over a larger area on the crystal surfaces, by making the first crystal severely asymmetric in the direction of

glancing incidence, and reversing the asymmetry with the second crystal. However, in this case the angular acceptance of the first crystal is substantially increased, hence the overall energy resolution greatly suffers.

Lastly, an option to consider is to cool both quartz crystals to cryogenic temperatures near 80 K. Then the thermal expansion of quartz is reduced by half, whereas its conductivity increases by about five times (Sutter & Yavas, 2017). All other parameters remaining unchanged would reduce the estimated rocking-curve broadening from  $\sim 14$  to  $\sim 1.7$ . For the present purpose, this improvement would still be insufficient but might be appropriate for less demanding applications.

Altogether, the considerations above lead us to believe that quartz at room temperature is not a good choice for X-ray optics such as high-resolution monochromators, when noticeable amounts of power as low as 100 mW are involved. In contrast, sapphire crystals showed only mild distortion under similar power conditions and are a much better choice for monochromator applications, although still inferior to Si optics.

### Funding information

This research used resources of the Advanced Photon Source, a US Department of Energy (DOE) Office of Science User

Facility operated for the DOE Office of Science by Argonne National Laboratory (under contract No. DE-AC02-06CH11357).

### References

- Ament, L. J. P., van Veenendaal, M., Devereaux, T. P., Hill, J. P. & van den Brink, J. (2011). *Rev. Mod. Phys.* **83**, 705–767.
- Authier, A. (2001). *Dynamical Theory of X-ray Diffraction, International Union of Crystallography Monographs on Crystallography*. Oxford University Press.
- Carslaw, H. S. & Jaeger, J.-C. (1959). *Conduction of Heat in Solids*. p. 214. Oxford University Press.
- DuMond, J. W. (1937). *Phys. Rev.* **52**, 872–883.
- Gog, T., Casa, D. M., Said, A. H., Upton, M. H., Kim, J., Kuzmenko, I., Huang, X. & Khachatryan, R. (2013). *J. Synchrotron Rad.* **20**, 74–79.
- Hönnicke, M. G., Huang, X., Cusatis, C., Koditwakk, C. N. & Cai, Y. Q. (2013). *J. Appl. Cryst.* **46**, 939–944.
- Kim, J., Casa, D., Said, A., Krakora, R., Kim, B. J., Kasman, E., Huang, X. & Gog, T. (2018). *Sci. Rep.* **8**, 1958.
- Said, A. H., Gog, T., Wiczorek, M., Huang, X., Casa, D., Kasman, E., Divan, R. & Kim, J. H. (2018). *J. Synchrotron Rad.* **25**, 373–377.
- Simmons, G. (1961). *J. Geophys. Res.* **66**, 2269–2270.
- Sutter, J. P., Baron, A. Q., Ishikawa, T. & Yamazaki, H. (2005). *J. Phys. Chem. Solids*, **66**, 2306–2309.
- Sutter, J. P., Baron, A. Q. R., Miwa, D., Nishino, Y., Tamasaku, K. & Ishikawa, T. (2006). *J. Synchrotron Rad.* **13**, 278–280.
- Sutter J. P. & Yavas H. (2017). *arXiv:1612.07049v2*.
- Yavaş, H., Sutter, J., Gog, T., Wille, H. -C. & Baron, A. Q. R. (2017). *MRS Bull.* **42**, 424–429.